MNRAS **000**, 1–12 (2015) Preprint 2 April 2016 Compiled using MNRAS LATEX style file v3.0

# Near-uniform internal rotation of the main sequence $\gamma$ Doradus pulsator KIC 7661054

Simon J. Murphy,[1,2]⋆ Luca Fossati,[3] Timothy R. Bedding,[1,2] Hideyuki Saio,[4] Donald W. Kurtz,[5] Luca Grassitelli,[6] Edric S. Wang[1]

[1] *Sydney Institute for Astronomy (SIfA), School of Physics, University of Sydney, NSW 2006, Australia*
[2] *Stellar Astrophysics Centre, Department of Physics and Astronomy, Aarhus University, 8000 Aarhus C, Denmark*
[3] *Space Research Institute, Austrian Academy of Sciences, Schmiedlstrasse 6, 8042 Graz, Austria*
[4] *Astronomical Institute, Graduate School of Science, Tohoku University, Sendai, Miyagi 980-8578, Japan*
[5] *Jeremiah Horrocks Institute, University of Central Lancashire, Preston PR1 2HE, UK*
[6] *Argelander-Institut für Astronomie, Universität Bonn, auf dem Hügel 71, 53121 Bonn, Germany*

Accepted XXX. Received YYY; in original form ZZZ

**ABSTRACT**

We used *Kepler* photometry to determine the internal rotation rate of KIC 7661054, a chemically normal $\gamma$ Dor star on the main sequence at spectral type F2.5 V. The core rotation period of $27.25 \pm 0.06$ d is obtained from the rotational splittings of a series of dipole g modes. The surface rotation period is calculated from a spectroscopic projected rotation velocity and a stellar radius computed from models. Literature data, obtained without inclusion of macroturbulence as a line-broadening mechanism, imply that the surface rotates much more quickly than the core, while our detailed analysis suggests that the surface may rotate slightly more quickly than the core and that the rotation profile is uniform within the 1-$\sigma$ uncertainties. We discuss the pitfalls associated with the determination of surface rotation rates of slow rotators from spectroscopy in the absence of asteroseismic constraints. A broad signal is observed at low frequency, which we show cannot be attributed to rotation, contrary to previous suggestions concerning the origin of such signals.

**Key words:** asteroseismology – stars: individual: KIC 7660154 – stars: oscillations – stars: rotation – techniques: spectroscopic

## 1 INTRODUCTION

The theories of stellar structure and evolution are triumphs of astrophysics over the last century. We now have a reasonable overview of the lives of single stars, from their formation out of the interstellar medium to their final death stages. In his classic text *The Internal Constitution of the Stars* Eddington (1926) warned in the introduction that "We should be unwise to trust scientific inference very far when it becomes divorced from the opportunity for scientific test", a warning that was particularly aimed at the inability in his time to see into the interiors of stars to test theories of structure and evolution. Now, with the expanding observational view of stellar interiors afforded by asteroseismology, we have alleviated Eddington's concern, and stellar physics that was once purely theoretical is now also observational.

The rotation of stars from their cores to their surfaces, and angular momentum transport mechanisms, both internal and external, significantly affect the structure and evolution of stars. We expect that stars are born with uniform rotation, as a consequence of thorough mixing throughout the star during the Hayashi contraction phase when the stars are fully convective. We further expect that, during evolution on the main sequence, conservation of angular momentum leads to a spin-up of the contracting core and a spin-down of the expanding envelope, leading to radially differential rotation. We also expect that internal energy transport mechanisms in rotating stars, which are not purely spherical, lead to latitudinal differential rotation.

These expectations can be tested with observations: from light modulations for latitudinal differential rotation at the surface and by asteroseismology for radial differential rotation with depth. The best-studied case is, of course, the Sun, where surface differential rotation has been known for centuries from sunspot studies, and interior rotation has been mapped about halfway down to the core by helioseismology (e.g., Schou et al. 1998, Thompson et al. 2003, Eff-Darwich et al. 2008). Yet the Sun's internal rotation is not as first expected: theory suggested rotation on cylinders, which is not the case; there is unexpected shear in the convection zone; and the inner

⋆ E-mail: murphy@physics.usyd.edu.au (SJM)

© 2015 The Authors

Sun seems to rotate rigidly, implying stronger angular momentum transport mechanisms than were anticipated.

In the last few years, we have begun to observe with asteroseismology the internal radial rotation profiles of stars from hydrogen-burning main-sequence phases (Kurtz et al. 2014; Pápics et al. 2015; Saio et al. 2015; Schmid et al. 2015; Triana et al. 2015), through to subgiant and red giant phases (Beck et al. 2012; Mosser et al. 2012; Deheuvels et al. 2012, 2014, 2015), and even on to the late evolutionary stages of subdwarf B stars (Van Grootel et al. 2009) and white dwarfs (Charpinet et al. 2009).

Overall, the results are surprising. The main-sequence stars observed so far are nearly rigid rotators. Red giant cores rotate much more slowly compared to their surfaces than expected, and white dwarfs have shed their interior angular momentum. The disparity, for example, between theoretical and observed rotation profiles of red giants is two orders of magnitude (Eggenberger et al. 2012; Marques et al. 2013; Cantiello et al. 2014). All of this indicates that some physics is missing in models of angular momentum transport in stellar interiors.

*Kepler* observations show that the problem already exists on the main sequence. Two asteroseismic studies of rotation in main-sequence A stars have yielded uniform profiles, with core-to-surface rotation period ratios $P_{\rm core}/P_{\rm surface} = 1.07$ (KIC 11145123, Kurtz et al. 2014) and 0.97 (KIC 9244992, Saio et al. 2015). Those stars are chemically normal but are unusual in having remarkably long rotation periods of 105 and 66 d, respectively. Preliminary analysis of the rotation profiles of two more A stars with much shorter rotation periods (near 10 d) give $P_{\rm core}/P_{\rm surface} \approx 1.3$ and 0.9 (Schmid et al. 2015). Meanwhile, a 1-$\sigma$ detection of counter-rotation in a main-sequence B star (KIC 10526294, Triana et al. 2015) appears to require even more elaborate angular momentum transport, but the observations are consistent with rigid rotation within 2 $\sigma$ and the star's rotation period is also remarkably long at $\sim 188$ d (Pápics et al. 2014). Internal gravity waves could be responsible for these uniform or even counter-rotating profiles (Rogers et al. 2013).

There is some evidence that the surface rotation rates of main-sequence A stars increase during the first third of their main-sequence lifetimes (Zorec & Royer 2012). Murphy (2014) found this counter-intuitive result to be corroborated by literature data (Wolff & Simon 1997; Erspamer & North 2003). The cause is the extra braking undergone at the surface during the pre-main-sequence phase (Stępień 2000), when a strong interaction with a proto-planetary disk limits spin-up of the stellar surface as the star contracts towards the zero-age main-sequence (ZAMS). This idea is supported by observations of pre-main-sequence A stars rotating at small fractions of their critical rotation velocity (Zwintz et al. 2014). However, the core is not as strongly affected by interaction with the proto-planetary disk, and at the ZAMS it is rotating more rapidly than the surface, slowly transferring angular momentum towards the surface as the star evolves on the main-sequence. It takes an A star a third of its main-sequence lifetime to reach an equilibrium (Zorec & Royer 2012).

The physics of angular momentum transport on the main sequence has been poorly constrained. Now that asteroseismology using ultra-precise space-based photometry offers observation of the stellar interior, efforts to examine the efficiency of various transport mechanisms have been renewed (Tayar & Pinsonneault 2013; Fuller et al. 2014).

Magnetism is one such angular momentum transport mechanism that has seen a recent revival of interest. Cantiello et al. (2014) showed that magnetic torques in radiative regions cannot single-handedly reproduce observed red giant rotation profiles (e.g. Beck et al. 2012), but they do play a significant role. Since then, magnetic dynamos in convective stellar cores have been suggested to be near-ubiquitous (Fuller et al. 2015; Stello et al. 2016). Intermediate-mass red giants are thought to have strong magnetic fields in their cores, generated when they were main-sequence A/F stars and their cores were convective. The magnetism is inferred to exist in 50 per cent of red giants with A-star progenitors, much larger than the fraction of A stars with global dipolar magnetic fields (5–10 per cent, Wolff 1983). The magnetic fields act like a greenhouse, trapping and scattering dipole oscillation-mode energy. If these magnetic greenhouses also affect angular momentum transport, they may explain the observed rotation profiles of some red giants. Further, since the magnetic fields develop on the main sequence, they may influence angular momentum transport there, too.

This work is part of an ongoing project to map the rotation profiles of main-sequence stars, providing much-needed observational results. The identification of consecutive radial orders of g modes in the light curves of A/F stars ($\gamma$ Dor stars) offers a measurement of the stellar age through their period spacings (Miglio et al. 2008). When these modes show clear multiplets, the core rotation rate can be determined. Period spacings have been detected in dozens of $\gamma$ Dor stars (Van Reeth et al. 2015a), but only a small number have evident rotational splittings (Bedding et al. 2015). Some $\gamma$ Dor stars also show p modes, which are sensitive to conditions at the surface. These $\delta$ Sct–$\gamma$ Dor hybrids offer an asteroseismic rotational profile from the core to the surface. In the absence of p modes, one must resort to spectroscopic rotational velocities.

In this paper we describe observations of g modes in KIC 7661054, revealing the core rotation rate of an F2.5V star on the main sequence (Sect. 2). Sect. 3 describes the process of obtaining the spectroscopic rotation velocity, and the treatment of various line broadening mechanisms. In Sect. 4 we describe the calculation of stellar models, using spectroscopic and asteroseismic information as constraints, in order to compute a stellar radius. This radius, when coupled with the surface rotation velocity, gives a rotation period for the surface. A discussion, which includes a description of the potential pitfalls in the methodology, is given in Sect. 5 before our conclusions in Sect. 6.

## 2 INVESTIGATING THE CORE ROTATION RATE WITH KEPLER PHOTOMETRY

We examined the full 1470.5 d of *Kepler* photometry available for KIC 7661054. The data have 29.43-min sampling, a duty cycle of 90.7 per cent, and were processed with the msMAP pipeline (Stumpe et al. 2012; Smith et al. 2012). We conducted our analysis with the frequency analysis package PERIOD04 (Lenz & Breger 2004, 2005) and our own tools. Fig. 1 shows the Fourier transform of the stellar light curve, revealing a series of g modes around 1 $\mathrm{d}^{-1}$, but an absence of p modes ($> 5\,\mathrm{d}^{-1}$).

KIC 7661054 shows a series of peaks with a roughly constant period spacing, typical of $\gamma$ Dor stars with slowly rotating cores (see, e.g., Bedding et al. 2015). An échelle diagram (Fig. 2) of these g modes shows an almost-complete series of dipole ($\ell = 1$) modes, split into doublets with $m = \pm 1$. The central ($m = 0$, zonal) component is weakly visible at four radial orders. The period spacings of these modes are shown in Fig. 3 and the g-mode dipole multiplets are identified in the Fourier transform in Fig. 4. Although the multiplets overlap, the rotational splittings and period spacings change only slowly with frequency, and correct identification is straightforward.

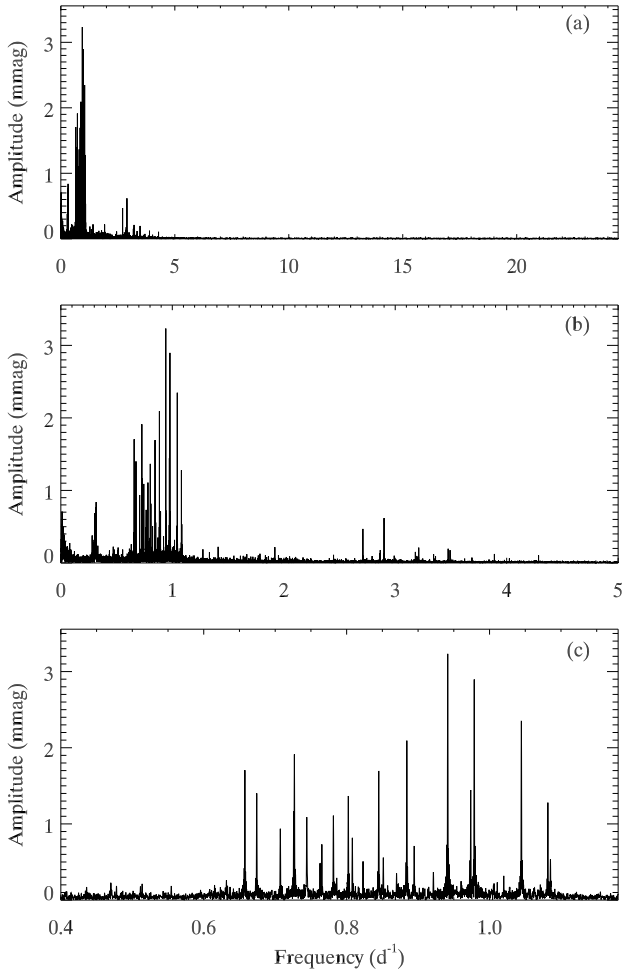


**Figure 1.** (a) Fourier transform of KIC 7661054 out to the Nyquist frequency of the *Kepler* data. (b) A zoom of the low-frequency region. The peaks at 0.3 d$^{-1}$ and at ~3 d$^{-1}$ are discussed in Sect. 5. (c) The series of dipole g mode oscillations.

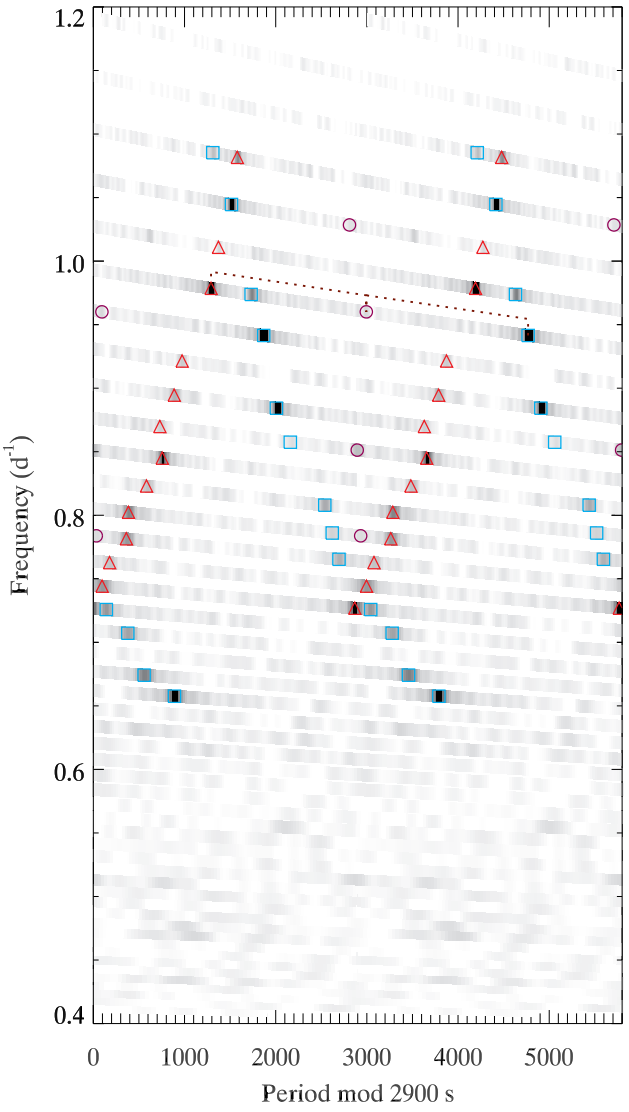


**Figure 2.** Échelle diagram for KIC 7661054 with period modulo 2900 s, plotted twice for clarity. The greyscale corresponds to Fourier amplitude. The frequency region displayed is the same as Fig. 1(c). The series on the outside of the diagram (triangles, left and squares, right) are the $m = +1$ and $m = -1$ modes, respectively. A weak series of zonal ($m = 0$) modes is visible as circles halfway between the $m = \pm 1$ modes at some orders. A dashed line identifies one of the dipole triplets.

The dipole modes have clear rotational splittings that we used to obtain the core rotation rate. Where available, we used the splittings between the $m = 0$ and $m = \pm 1$ modes of each radial order. For the orders where no $m = 0$ modes are observed, we took half the splitting of the $m = -1$ and $m = +1$ modes, instead. The splittings are shown as a function of frequency in Fig. 5. At radial orders where all three azimuthal components are observed, we note that the frequency splittings of the dipole modes are equal to within $\sim 2 \times 10^{-5}$ d$^{-1}$ after the overall trend with frequency is accounted for (see below). Frequency values are given in Table 1, along with amplitudes and uncertainties that show that each of the identified g modes has an amplitude of at least ~10 times the rms noise.

The rotation period of the core is given by (e.g. Aerts et al. 2010)

$$P_{\rm c} = \frac{1 - C_{n,l}}{\overline{\delta\nu}}, \qquad (1)$$

where $\overline{\delta\nu}$ is the mean observed frequency splitting of the g modes. These splittings change as a function of frequency (Fig. 5) because we are observing many radial orders and the Ledoux 'constant', $C_{n,l}$, is not strictly constant but depends on $n$ (e.g. Keen et al. 2015). Our asteroseismic models (described in Sect. 4) indicate a mean $C_{n,l}$ of 0.4952 for the radial orders observed. ($C_{n,l}$ changes from 0.4960 to 0.4943 over the observed frequency range.) For KIC 7661054 we obtain a core rotation frequency of 0.036696 ± 0.000080 d$^{-1}$ and a corresponding period of $P_{\rm c} = 27.25 \pm 0.06$ d. Bedding et al. (in prep.) are preparing a full characterisation of the change of $C_{n,l}$ with $n$ over many stars.

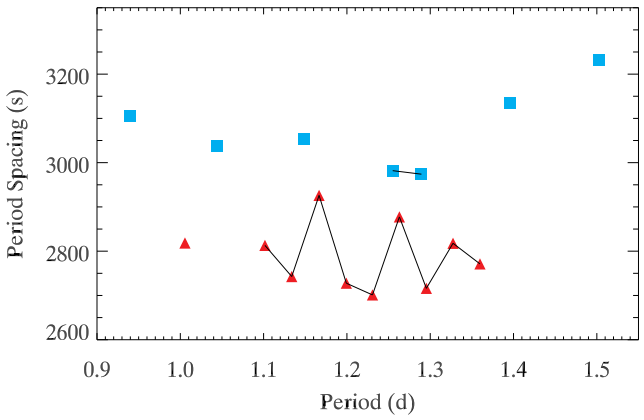


**Figure 3.** Period spacings of dipole g modes in KIC7661054. Lines connect neighbouring period spacings. Triangles and squares represent $m = +1$ and $m = -1$ modes, respectively.

**Table 1.** Identified modes in KIC 7661054, with frequencies, amplitudes and phases determined by non-linear least-squares fitting. The final column gives the azimuthal order; $\ell = 1$ for all modes.

| Frequency $d^{-1}$ | Amplitude mmag ±0.014 | Phase $[-\pi \,..\, \pi]$ | m |
|---|---|---|---|
| 0.470082 ± 0.000027 | 0.204 | −2.170 ± 0.070 | −1 |
| 0.513711 ± 0.000026 | 0.207 | −1.029 ± 0.069 | −1 |
| 0.554574 ± 0.000032 | 0.165 | −0.697 ± 0.087 | −1 |
| 0.657586 ± 0.000003 | 1.648 | 1.451 ± 0.009 | −1 |
| 0.674174 ± 0.000004 | 1.440 | −3.081 ± 0.010 | −1 |
| 0.707168 ± 0.000006 | 0.908 | 0.484 ± 0.016 | −1 |
| 0.725795 ± 0.000007 | 0.822 | −1.661 ± 0.018 | −1 |
| 0.765319 ± 0.000008 | 0.659 | −2.840 ± 0.022 | −1 |
| 0.786025 ± 0.000023 | 0.239 | −2.928 ± 0.060 | −1 |
| 0.807943 ± 0.000007 | 0.720 | −1.831 ± 0.020 | −1 |
| 0.857481 ± 0.000027 | 0.203 | 2.146 ± 0.071 | −1 |
| 0.884270 ± 0.000003 | 2.100 | 0.763 ± 0.007 | −1 |
| 0.941498 ± 0.000002 | 3.281 | 1.019 ± 0.004 | −1 |
| 0.973740 ± 0.000004 | 1.446 | −2.308 ± 0.010 | −1 |
| 1.044547 ± 0.000002 | 2.397 | 0.154 ± 0.006 | −1 |
| 1.085289 ± 0.000010 | 0.550 | −2.025 ± 0.026 | −1 |
| 0.783800 ± 0.000029 | 0.182 | −0.876 ± 0.080 | 0 |
| 0.851280 ± 0.000009 | 0.577 | 0.756 ± 0.025 | 0 |
| 0.960064 ± 0.000024 | 0.221 | −1.923 ± 0.065 | 0 |
| 1.028453 ± 0.000033 | 0.161 | −1.622 ± 0.089 | 0 |
| 0.726863 ± 0.000003 | 1.772 | 1.462 ± 0.008 | 1 |
| 0.744213 ± 0.000005 | 1.134 | −2.771 ± 0.013 | 1 |
| 0.762726 ± 0.000010 | 0.514 | 2.725 ± 0.028 | 1 |
| 0.781463 ± 0.000005 | 1.110 | 1.345 ± 0.013 | 1 |
| 0.802344 ± 0.000004 | 1.291 | −0.538 ± 0.011 | 1 |
| 0.822989 ± 0.000012 | 0.462 | 1.526 ± 0.031 | 1 |
| 0.844942 ± 0.000003 | 1.711 | 1.430 ± 0.008 | 1 |
| 0.869832 ± 0.000015 | 0.348 | −0.883 ± 0.041 | 1 |
| 0.894532 ± 0.000008 | 0.715 | 0.693 ± 0.020 | 1 |
| 0.921367 ± 0.000016 | 0.331 | 1.759 ± 0.043 | 1 |
| 0.978584 ± 0.000002 | 2.929 | −0.528 ± 0.005 | 1 |
| 1.010853 ± 0.000022 | 0.244 | 1.834 ± 0.059 | 1 |
| 1.081646 ± 0.000004 | 1.195 | 1.187 ± 0.012 | 1 |

## 3 PARAMETER DETERMINATION AND ABUNDANCE ANALYSIS

### 3.1 Overview

KIC 7661054 was observed on two separate nights in 2013 using the HERMES spectrograph on the Mercator Telescope by Niemczura et al. (2015, 'N15' hereafter). They analysed the spectra and provided atmospheric parameters that identified KIC 7661054 as a slow rotator ($v \sin i = 16 \pm 1\,\mathrm{km\,s^{-1}}$). Using those parameters, Murphy et al. (2015) showed KIC 7661054 to lie in the middle of the $\gamma$ Dor instability strip, and at the red edge of the $\delta$ Sct instability strip. The pulsation frequency distribution in Fig. 1 is consistent with this.

Note that the analysis by N15 did not incorporate macroturbulence. As they warned, neglecting macroturbulence can lead to a gross overestimate of $v \sin i$ in slow rotators. Macroturbulence is a significant line-broadening mechanism in late-A and early-F stars associated with a surface velocity field that can be as high as the local sound speed (Grassitelli et al. 2015). In the case of KIC 7661054, this is a large fraction of the published $v \sin i$ value. We therefore reanalysed the HERMES spectra, taking macroturbulence into account.

### 3.2 New analysis

#### *3.2.1 Line broadening – $v \sin i$ and $v_{\mathrm{macro}}$*

We computed model atmospheres of KIC 7661054 using the LLmodels stellar model atmosphere code (Shulyak et al. 2004). Local Thermodynamical Equilibrium (LTE) and plane-parallel geometry were assumed for all the calculations. We used the VALD database (Piskunov et al. 1995; Kupka et al. 1999) as a source of atomic line parameters for opacity calculations and convection was implemented according to the Canuto & Mazzitelli (1991, 1992) treatment.

We derived the projected rotational velocity ($v \sin i$) and macroturbulence velocity ($v_{\mathrm{macro}}$) using both line-profile fitting and Fourier analysis (Gray 2005). We first used the Fourier analysis of 27 unblended lines of various ions to estimate the $v \sin i$ value, obtaining an average of $v \sin i = 6.1 \pm 1.0\,\mathrm{km\,s^{-1}}$, where the uncertainty is the standard deviation from the mean value. For this analysis we adopted a fixed limb-darkening coefficient of 0.6 (Gray 2005). Figure 6 shows the Fourier amplitude as a function of $v \sin i$ for a sub-sample of six analysed metal-line profiles. For each line, the position of the first (leftmost) minimum indicates the best fitting $v \sin i$ value. It is important to note that our analysis strictly rules out $v \sin i > 10\,\mathrm{km\,s^{-1}}$.

To estimate $v_{\mathrm{macro}}$ we compared the Least Squares Deconvolution (LSD; Donati et al. 1997; Kochukhov et al. 2010) profile of the observed spectrum with LSD profiles of synthetic spectra calculated with SYNTH3 (Kochukhov 2007). These synthetic spectra were first broadened with a fixed $v \sin i$ value of $6.1\,\mathrm{km\,s^{-1}}$ and a $v_{\mathrm{macro}}$ variable between 0 and $15\,\mathrm{km\,s^{-1}}$. The $\chi^2$ analysis gave a best fitting $v_{\mathrm{macro}}$ value of $11 \pm 1\,\mathrm{km\,s^{-1}}$. For the calculation of the LSD profiles we adopted a line mask composed of only Fe lines (Reiners & Schmitt 2003) deeper than 0.1 from the continuum, and extracted from the VALD database using the final adopted atmospheric parameters and abundances (see below). The main advantage of using LSD profiles is the great increase in signal-to-noise ratio (S/N). This highlighted the slight asymmetry in the line profiles, as shown in Fig. 7, with the red wing being slightly broader than the blue wing. This asymmetry probably affects measurements

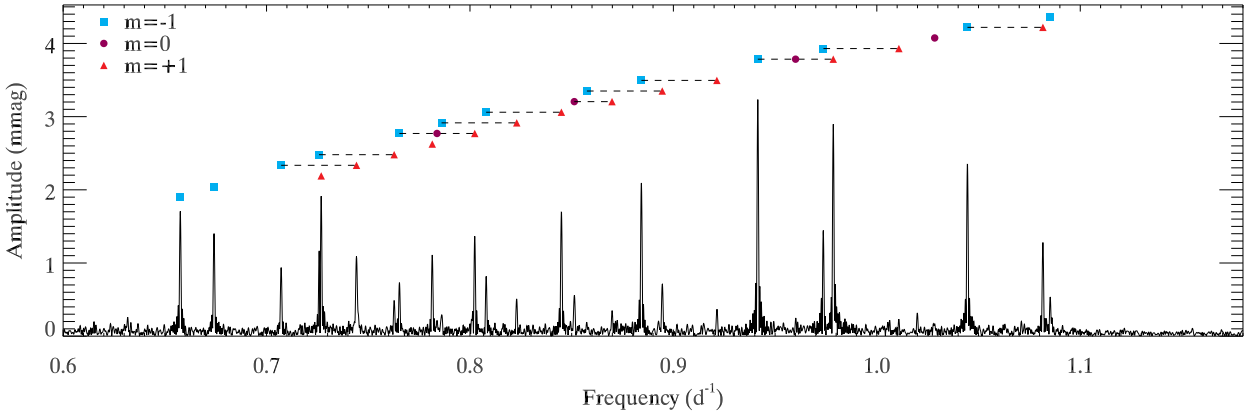


**Figure 4.** Identification of rotationally split dipole g modes in KIC 7661054.

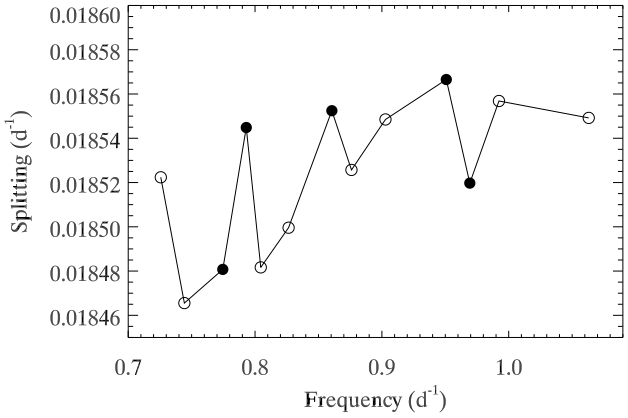


**Figure 5.** Rotational splittings of the g modes. Filled symbols denote splittings between zonal modes ($m = 0$) and sectoral modes ($m = +1, -1$), whereas open symbols are the splittings between $m = +1$ and $m = -1$ modes, halved. Points are connected to guide the eye, only. Frequency uncertainties are of the order $1 \times 10^{-5}$d$^{-1}$.

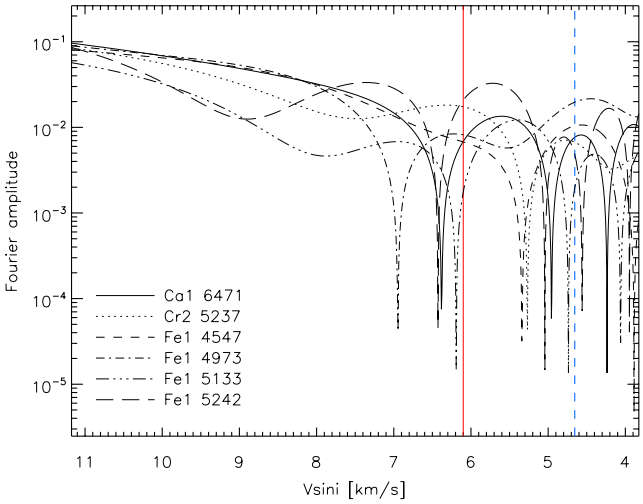


**Figure 6.** Amplitude of the Fourier transform (in log scale) of six analysed metal line profiles as a function of $v \sin i$. The position of the first minimum indicates the $v \sin i$ value. The vertical solid (red) and dashed (blue) lines indicate respectively the final adopted $v \sin i$ value and the resolution limit. The legend indicates the ion and approximate wavelength (in Å) of the considered transitions.

of $v \sin i$, and therefore $v_{\rm macro}$ (see, e.g., Aerts et al. 2014), hence the true uncertainties may be slightly larger than those given here.

### 3.2.2 *Global parameters – $T_{\rm eff}$, $\log g$ and [Fe/H]*

The evaluation of the aforementioned line-broadening mechanisms in KIC 7661054 results in substantially different line profiles from those of N15. Their spectral synthesis is therefore incompatible with the present analysis, so we re-derived all of the atmospheric parameters, as well as abundances for 23 elements.

In the temperature range in which KIC 7661054 lies, the hydrogen line wings are sensitive almost exclusively to effective temperature ($T_{\rm eff}$) variations. To spectroscopically derive $T_{\rm eff}$ from hydrogen lines, we fitted synthetic line profiles to the observed H$\alpha$, H$\beta$, and H$\gamma$ Balmer line profiles. Note that SYNTH3 incorporates the code by Barklem et al. (2000)[1], which takes into account not only self-broadening but also Stark broadening (see their Sect. 3).

[1] `http://www.astro.uu.se/~barklem/hlinop.html`

Figure 8 compares the observed hydrogen line profiles with two synthetic profiles, one calculated with our final set of parameters, and the other with the set of parameters from N15. The synthetic spectrum corresponding to our final model does not perfectly fit the hydrogen line profiles; this would require a slightly lower temperature by ~50–100 K, which is ruled out by analysis of the metal lines (see below). The difference between our final synthetic and observed profiles can be attributed to normalisation, which is always challenging for hydrogen lines observed with échelle spectra (Fossati et al. 2011), and to three dimensional effects (Cayrel et al. 2011), which are not taken into account in our 1D model.

The surface gravity ($\log g$) was derived from two independent methods based on the line-profile fitting of the Mg I b triplet and the ionisation balance for several elements. The first method, as described by Fuhrmann et al. (1997), is based on the fact that the wings of the Mg I lines at $\lambda$ 5167, 5172, and 5183 Å are sensitive

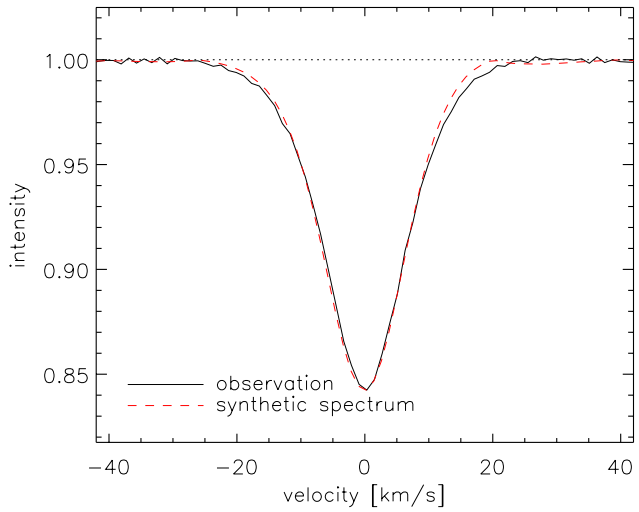


**Figure 7.** Comparison between the LSD profiles of the observed spectrum (black solid line) and of the synthetic spectrum (red dashed line) calculated with the final adopted atmospheric parameters (including $v \sin i$ and $v_{\rm macro}$) and abundances. The comparison shows the presence of a slight asymmetry in the LSD profile of the observed spectrum.

to $\log g$ variations. To estimate $\log g$ from the Mg I lines we used the Mg abundance obtained from the Mg I line at $\lambda$ 5711 Å, which shows little dependence on non-LTE effects (Fossati et al. 2011) and then tuned the $\log g$ value to fit the line wings. For this operation we adopted the $v \sin i$ and $v_{\rm macro}$ values described above and the microturbulence velocity ($v_{\rm mic}$) obtained by requiring no correlation between the line abundance and equivalent width for several ions (see below).

To derive $\log g$ from the fit of the Mg I lines with extended wings we adopted the $\log(gf)$ and damping constants used by Ryabchikova et al. (2016) for the analysis of a sample of benchmark F-, G- and K-type main sequence stars. The middle panel of Fig. 9 compares the observed spectrum of KIC 7661054 in the region of the Mg I 5172 and 5183 Å lines with synthetic spectra calculated with the final adopted parameters and those of N15.

Figure 9 shows a good agreement between the synthetic profiles calculated with our final adopted parameters and the observed spectrum. On the other hand, the synthetic profiles calculated with N15's parameters do not agree with the observations, mostly caused by neglecting macroturbulent broadening and hence overestimating $v \sin i$.

The metallic-line spectrum provides further constraints on the atmospheric parameters. If we assume no deviation from LTE, there should be no trend in individual line abundances as a function of excitation potential. Examining this for any ion provides a measurement of $T_{\rm eff}$. The balance between different ionisation stages of the same element similarly provides a measurement of $\log g$, while $v_{\rm mic}$ is determined by minimising any trend between individual line abundances and equivalent widths for a certain ion. Determining the fundamental parameters in this way must be done iteratively since, for example, a variation in $T_{\rm eff}$ leads to a change in the best $\log g$ and $v_{\rm mic}$ values (Fossati et al. 2011).

LTE line abundances were based on equivalent widths[2], analysed with a modified version (Tsymbal 1996) of the WIDTH9 code (Kurucz 1993). For all measured transitions, we adopted the line parameters given by the VALD database. In practice, it was not possible to get unique $T_{\rm eff}$, $\log g$ and $v_{\rm mic}$ values for all considered species, therefore we calculated values that best satisfy all the data, leaving minimal scatter.

Taking into account all parameter indicators, we finally adopted $T_{\rm eff} = 6800 \pm 100$ K, $\log g = 3.7 \pm 0.1$, and $v_{\rm mic} = 2.4 \pm 0.2$ km s$^{-1}$. With these parameters we obtained an iron abundance of [Fe/H] $= -0.12 \pm 0.12$ dex. These parameters all agree at $1\sigma$ with those of N15, except for the surface gravity, which disagrees by $3\,\sigma$. We checked the impact of adopting a higher surface gravity in our analysis: it leads to a significantly worse ionisation equilibrium for several elements and a poorer fit of the Mg I line profiles.

The full set of derived abundances, referenced to solar abundances from Asplund et al. (2009), is given in Table 2. The abundance uncertainties given in Table 2 are the standard deviation from the mean abundance. The abundances do not take into account hyperfine structure effects, hence the abundances of elements such as Mn and Cu have to be taken with caution. We did not use ions that may be significantly affected by hyperfine structure effects for the derivation of the atmospheric parameters.

## 4 STELLAR MODELS AND SURFACE ROTATION

### 4.1 Rotation of the surface

In the absence of p modes in KIC 7661054, we cannot determine a surface rotation frequency from asteroseismology. Instead, the spectroscopic $v \sin i$ can be used to calculate the surface rotation rate with a suitable estimate of the stellar radius, albeit with the inclination value unknown.

#### 4.1.1 *Estimate of the radius*

We used the spectroscopic parameters, with the additional constraint of the g-mode period spacings, to model the star. Evolutionary models were calculated using the Modules of Experiments in Stellar Evolution (MESA) code (Paxton et al. 2013). We adopted a solar composition of $X = 0.72$, $Z = 0.014$, in accordance with the spectroscopic abundances given in Table 2.

Diffusive overshooting implemented in the MESA code was adopted, in which the mixing efficiency is assumed to decay exponentially as $\exp[-2z/(h_{\rm ov} H_p)]$ with $z$ being the distance from the boundary of the convective core (Herwig 2000). The extent of overshooting in evolutionary models is controlled by the free parameter $h_{\rm ov}$.[3] The main-sequence band in the HR diagram is wider for models with larger $h_{\rm ov}$ (Fig. 10). An appropriate value of $h_{\rm ov}$ can be obtained by using the g-mode period spacings combined with the spectroscopic parameters $T_{\rm eff}$ and $\log g$.

Period spacings of g modes in a main-sequence star generally decrease as the star evolves (Fig. 11). The models of period spacings correspond to $m = 0$ modes, whereas the consecutive orders of g modes in KIC 7661054 are best seen in the $m = +1$ modes. We therefore transformed the $m = +1$ modes to values consistent with the (unseen) $m = 0$ modes by subtracting the rotation frequency in accordance with a linear fit to the frequency splittings in Fig. 5.

[2] Note that equivalent widths are unaffected by $v \sin i$ or $v_{\rm macro}$ broadening.

[3] An alternative way to include overshooting is to fully mix the zone of thickness $\alpha_{\rm ov} H_p$ above the convective core boundary. It is known empirically that similar models are obtained by substituting $h_{\rm ov}$ with $0.1\alpha_{\rm ov}$.

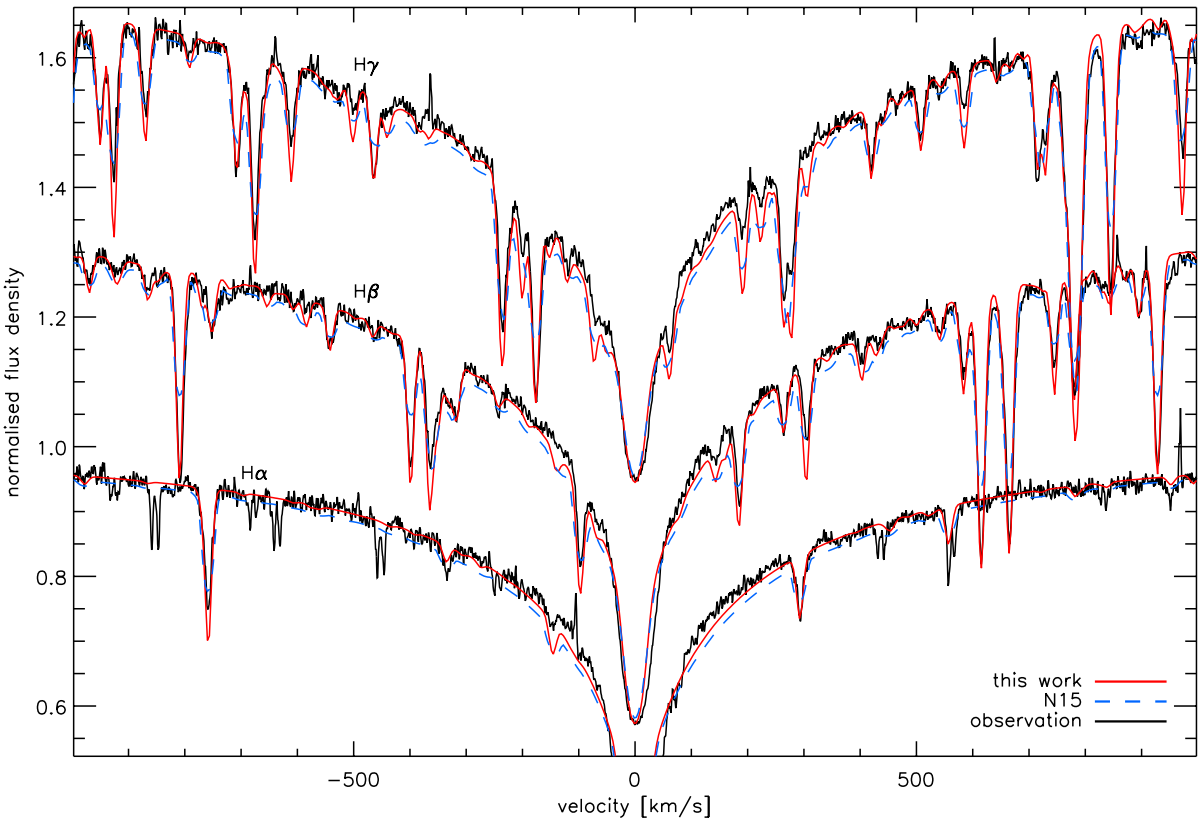


**Figure 8.** Comparison between the observed line profiles (solid black lines) of H$\alpha$ (bottom), H$\beta$ (middle), and H$\gamma$ (top) and synthetic profiles calculated with our final adopted parameters (solid red lines) and with the parameters given by N15 (dashed blue lines). The wavelengths are converted to velocities and brought to the rest frame of each considered Balmer line, so that the centre of each line is at 0 km s$^{-1}$. The profiles are vertically offset for clarity.

Along each evolutionary track for a given parameter set, there exists a stage at which the period spacings of high-order g modes are consistent with the observed ones of KIC 7661054. These stages are shown by open circles in Fig. 10. This figure indicates that the spectroscopic parameters ($T_{\rm eff}$, $\log g$) of KIC 7661054 are consistent with the stage of 1.9 M$_\odot$ with $h_{\rm ov} = 0.015$ (i.e., $\alpha_{\rm ov} \approx 0.15$).

In summary, our best model has a core hydrogen fraction $X_c = 0.11 \pm 0.01$ at $M = 1.9\,{\rm M}_\odot$, and a radius $R = 3.2\,{\rm R}_\odot$. The core overshooting is constrained to $h_{\rm ov} \approx 0.015$ ($\alpha_{\rm ov} \approx 0.15$).

The results are very sensitive to the spectroscopic $\log g$. The uncertainty on the stellar radius is based on this $\log g$, and equals 0.4 R$_\odot$. Attempts to use the asteroseismic period spacings to refine this uncertainty are hindered by the number of free parameters in the models. That is, the observed period spacings can be matched with models within the spectroscopic error box by making small changes to the mass, overshooting and/or metallicity of the model. The stellar radius is constrained by the spectroscopic $\log g$, and is relatively insensitive to 1-$\sigma$ changes to the metallicity of the models.

### 4.1.2 *Calculating surface rotation*

If the inclination is 90° then the radius of $3.2 \pm 0.4\,{\rm R}_\odot$ and $v \sin i = 6.1 \pm 1.0$ km s$^{-1}$ imply a surface rotation period of $P_{\rm s} = 26.7 \pm 4.7$ d. Comparison with the core rotation period, $P_{\rm c} = 27.25 \pm 0.06$ d, reveals a ratio consistent with uniform (solid-body) rotation. If the inclination is less than 90° then the derived surface rotation period is shorter. Hence uniform rotation is implied at the upper limit of the surface rotation period, only.

There is some evidence that favours a near-equatorial aspect. In $\gamma$ Dor stars, equipartition of energy probably does not hold exactly because of the nature of the driving mechanism, but the principles of partial cancellation of non-radial modes across the integrated stellar disk still apply. Thus the detection of $m = 0$ modes, regardless of their amplitudes, rules out $i = 90°$, and the dominance of $|m| = 1$ modes suggests $i >> 0°$.

If energy were approximately equipartitioned, the amplitude ratios of the multiplets would suggest a nearly equator-on aspect because many sectoral ($|m| = 1$) modes are observed compared with only four weak zonal ($m = 0$) modes (Gizon & Solanki 2003). At radial orders where all three azimuthal components are observed, the amplitude ratios ($A_{|m|=1}/A_{m=0}$) range from 4 to 15.

The median value of the inclination for a randomly distributed ensemble is $i = 60°$. The apparent dominance of sectoral modes over zonal modes suggests that $i$ is much closer to 90° than to 0°, so we infer that $60° \lesssim i \lesssim 80°$, but this is not at all certain. Surface rotation periods for those angles are $P_{\rm s} = 23.1 \pm 4.1$ and $26.3 \pm 4.6$ d, respectively. Thus, while the surface nominally appears to rotate more quickly than the core, the observations remain consistent with uniform rotation at the 1-$\sigma$ level.

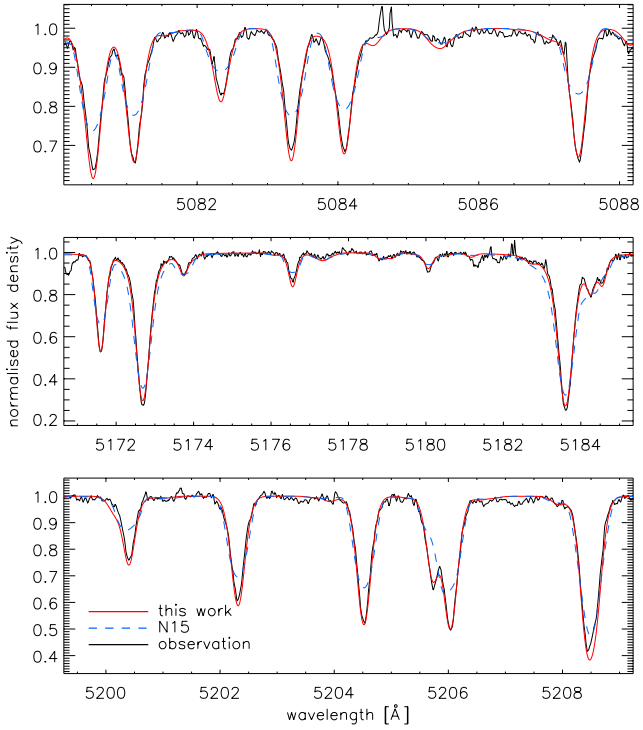


**Figure 9.** Comparison between the observed spectrum of KIC 7661054 (black solid line) and synthetic spectra calculated with our final adopted parameters (red solid line) and with the parameters adopted by N15 (blue dashed line) in three different wavelength regions covering metal lines. The middle panel shows the Mg I 5172 and 5183 Å line profiles adopted as log $g$ indicators.

## 5 DISCUSSION

### 5.1 Additional line broadening mechanisms

The high-order, non-radial pulsations seen in $\gamma$ Dor stars are a large contributor to spectral line broadening. The velocity field arising from pulsation is equivalent to macroturbulence – motion on a scale larger than the line forming region (Aerts et al. 2009; Simón-Díaz & Herrero 2014). Hence, pulsational broadening is taken into account via our macroturbulence term. In other words, some of the $v_{\rm macro}$ we measured actually arises from the g-mode pulsations, while some most likely originates from turbulence in the convective zones (Grassitelli et al. 2015).

The line-profile asymmetry shown in Fig. 7 affects, to some extent, the derived values for $v_{\rm macro}$ and $v \sin i$. This is especially true in the case of low projected rotational velocities, and most likely indicates the presence of surface spots or density inhomogeneities (Aerts et al. 2014). This fact, along with the uncertainties in the atmospheric parameters, explains the slight deviations in our $v_{\rm macro}$ value ($11 \pm 1$ km s$^{-1}$) from the prediction of Grassitelli et al. (2015, 9.8 km s$^{-1}$), though the two values are only 1 $\sigma$ different.

For confirmation that pulsations are not causing substantial distortion of the line profiles, we looked for line-profile variations (LPVs) in our spectra. The four available spectra were taken in two pairs: one pair in 2013 July and the other in 2013 September. For each of the four spectra we analysed four spectral lines of Fe I (Fig. 12), which are those chosen by Zima et al. (2006) for the $\delta$ Sct star FG Vir. The relative separation of the spectra in time is indicated in the left-centre panel of Fig. 12, and the zero point is the time of the mid-point of the first spectrum. Integration times were ~30 min, which is much shorter than the oscillation periods of ~1 d. There are some temporal changes in the observed line profiles, but they are not the same for each line, indicating that if any pulsational LPVs do exist then they are buried in the noise.

The *Kepler* light curve is unremarkable at the times during which the spectra were taken – the pulsational variability was not particularly strong (light curve maxima of 5 mmag, compared to 15 mmag at other times), and the brightness was close to the mean (displacements of −3 to +4 mmag).

In Appendix A we examine the amount of pulsational broadening (strictly, the magnitude of the horizontal motion) that is to be expected from g modes of a certain light amplitude. The averaged contribution is between 2 and 3 km s$^{-1}$.

This work has highlighted the difficulty in using spectroscopic $v \sin i$ measurements to infer surface rotation periods. Many factors can affect the profiles of spectral lines and, if significant broadening

**Table 2.** LTE atmospheric abundances for KIC 7661054 with error bar estimates based on the internal scatter from the number of analysed lines, $n$. The penultimate column gives the solar abundance values from Asplund et al. (2009), and the final column gives the elemental abundance with respect to those solar values. The uncertainties on those values are the same as in the second column.

| Ion | KIC 7661054 | | Sun | [*El.*/H] |
|---|---|---|---|---|
| | log($N/N_{\rm tot}$) | $n$ | log($N/N_{\rm tot}$) | |
| C I | −3.71 ± 0.12 | 9 | −3.61 | 0.10 |
| N I | −4.14 | 1 | −4.21 | −0.07 |
| O I | −3.36 | 1 | −3.35 | 0.01 |
| Na I | −5.77 ± 0.15 | 2 | −5.80 | −0.03 |
| Mg I | −4.61 | 1 | −4.44 | 0.17 |
| Si I | −4.74 ± 0.07 | 13 | −4.53 | 0.21 |
| Si II | −4.48 ± 0.11 | 4 | −4.53 | −0.05 |
| S I | −4.98 | 1 | −4.92 | 0.06 |
| K I | −6.59 | 1 | −7.01 | −0.42 |
| Ca I | −5.83 ± 0.04 | 10 | −5.70 | 0.13 |
| Ca II | −5.58 ± 0.05 | 3 | −5.70 | −0.12 |
| Sc II | −8.86 ± 0.09 | 6 | −8.89 | −0.03 |
| Ti I | −7.40 ± 0.06 | 3 | −7.09 | 0.31 |
| Ti II | −7.28 ± 0.11 | 8 | −7.09 | 0.19 |
| Cr I | −6.59 ± 0.14 | 10 | −6.40 | 0.19 |
| Cr II | −6.28 ± 0.02 | 6 | −6.40 | −0.12 |
| Mn I | −6.81 ± 0.04 | 3 | −6.61 | 0.20 |
| Fe I | −4.73 ± 0.12 | 148 | −4.54 | 0.19 |
| Fe II | −4.57 ± 0.06 | 25 | −4.54 | 0.03 |
| Co I | −7.20 | 1 | −7.05 | 0.15 |
| Ni I | −5.83 ± 0.06 | 34 | −5.82 | 0.01 |
| Cu I | −8.03 ± 0.01 | 2 | −7.85 | 0.18 |
| Zn I | −7.68 | 1 | −7.48 | 0.20 |
| Y II | −9.72 ± 0.06 | 5 | −9.83 | −0.11 |
| Zr II | −9.20 | 1 | −9.46 | −0.26 |
| Ba II | −9.88 | 1 | −9.86 | 0.02 |
| Ce II | −10.40 ± 0.01 | 2 | −10.46 | −0.06 |
| Nd II | −10.42 | 1 | −10.62 | −0.20 |
| $T_{\rm eff}$ [K] | 6800 ± 100 | | 5777 | |
| log $g$ | 3.7 ± 0.1 | | 4.44 | |
| $v_{\rm mic}$ [km s$^{-1}$] | 2.4 ± 0.2 | | 0.875 | |
| $v \sin i$ [km s$^{-1}$] | 6.1 ± 1.0 | | 1.6 | |
| $v_{\rm macro}$ [km s$^{-1}$] | 11 ± 1.0 | | 1.8 | |
| [Fe/H] | −0.12 ± 0.12 | | 0.0 | |

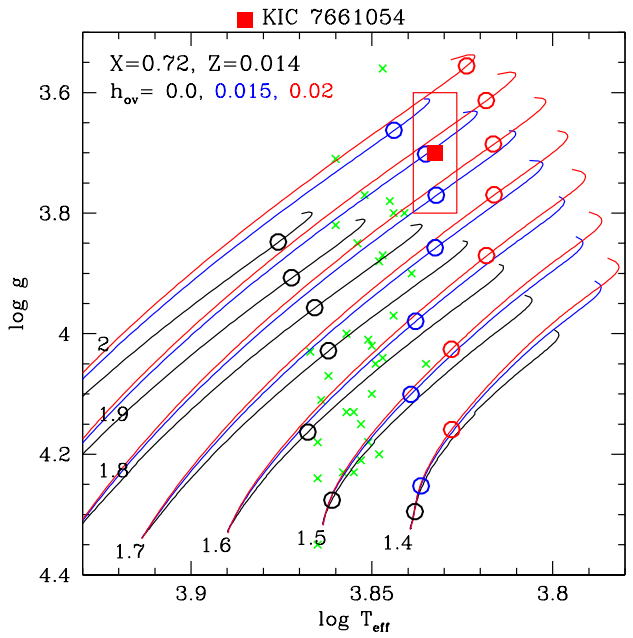


**Figure 10.** Evolutionary tracks with and without core overshooting. The extent of the overshooting is parameterized by $h_{\rm ov}$, which is approximately $0.1\alpha_{\rm ov}$. Tracks are labelled with masses in units of $M_\odot$. The 1-sigma spectroscopic constraints for KIC 7661054 are illustrated with the red rectangle. Circles indicate positions where the observed period spacings match the computed ones, leaving a clear solution described in the text. Other $\gamma$ Dor stars from Van Reeth et al. (2015a) are shown as green crosses.

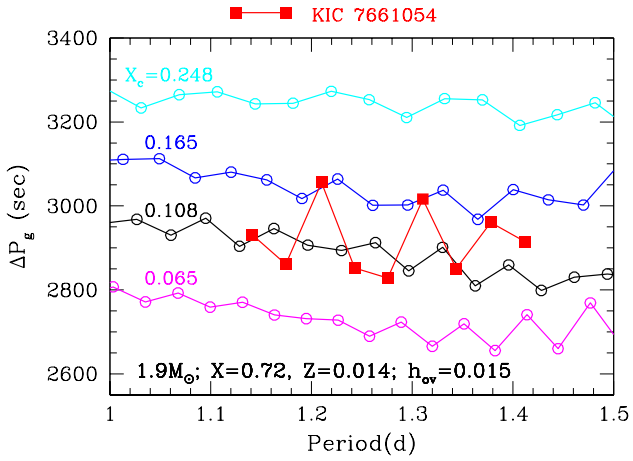


**Figure 11.** Period spacings of g modes as a function of period for selected models of $1.9\,M_\odot$ ($h_{\rm ov} = 0.015$) are compared with the relation for $m = 0$ modes of KIC 7661054 (connected red squares, transformed from $m = 1$ modes by subtracting the rotation). Each model relation is labelled by its central hydrogen abundance, $X_{\rm c}$.

mechanisms are omitted from consideration, then the $v \sin i$ value derived can be grossly incorrect. The best fitting stellar evolution models are highly dependent on the adopted spectroscopic parameters used as inputs, which themselves depend on the treatment of broadening mechanisms.

To illustrate this point, we briefly consider the $P_{\rm c}/P_{\rm s}$ ratio for KIC 7661054 that would be obtained by taking the spectroscopic values from N15 at face value. The stellar radius we obtained from

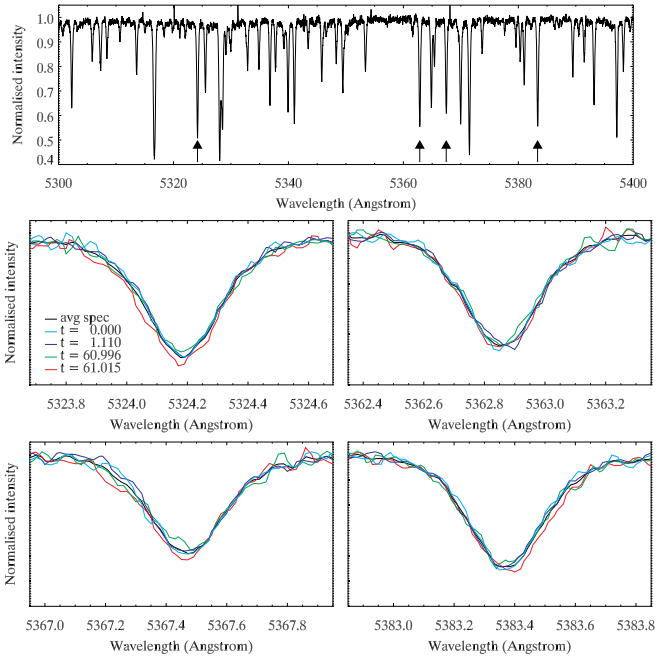


**Figure 12.** Line profile variation analysis for four lines of Fe I, which are identified in the top panel and shown close-up in subsequent panels. Comparison of individual spectra (coloured lines) to the average spectrum (black lines) shows no significant time-dependent line profile variation. The relative separations of the mid-observation time for each spectrum are provided in the centre-left panel (in units of d).

models with their $\log g (= 4.0)$ is $2.1\,R_\odot$. When used with their $v \sin i = 16\,{\rm km\,s^{-1}}$ the inferred surface rotation period is just 7 d, which leads to a $10\,\sigma$ detection of the core rotating more slowly than the envelope, with $P_{\rm c}/P_{\rm s} = 4$.

Finally, we remark that an abundance of free parameters in stellar evolution models – particularly the extent of core overshoot – can lead to a poorly constrained stellar radius, on which the surface period depends.

## 5.2 Additional peaks in the Fourier transform

### *5.2.1 At 3 $d^{-1}$ – low-order g modes?*

We noted in Fig. 1 the presence of peaks near $3\,{\rm d}^{-1}$. They are much higher in frequency than the main series of g modes and do not appear to be equally spaced in period. We also do not find common frequency splittings among any of the strongest (>0.08 mmag) peaks in this region.

We considered that these peaks could be lower-order g modes. The main series (Figs 1c, 2 & 3) contains g modes with radial orders[4] of −30 to −40. If the 3-$d^{-1}$ peaks are also g modes in the same star, they would have radial orders of around −10 for $\ell = 1$ or −17 for $\ell = 2$. Note that $\ell = 2$ modes have been observed in $\gamma$ Dor stars (Bedding et al. 2015; Keen et al. 2015), but our models do not predict these orders to be excited with the conventional driving mechanism in KIC 7661054, and the apparent absence of period spacings or frequency splittings disfavours the $\ell = 2$ hypothesis.

Another possibility is that these are combination modes, e.g.

[4] The radial orders of g modes are usually denoted with negative numbers.

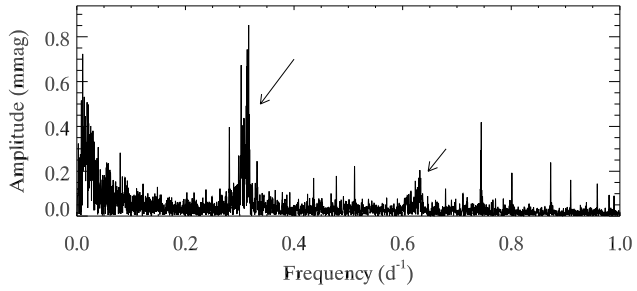


**Figure 13.** The Fourier residuals after a non-linear least-squares fit to the dipole g modes. Arrows indicate the feature discussed in the text and its harmonic.

$\nu_k = \nu_i + \nu_j$, which are known to exist in g mode pulsators (Kurtz et al. 2015; Van Reeth et al. 2015b). This possibility cannot be definitively ruled out because a large number of potential parent modes allows virtually any peak to be explained as a linear combination, but the absence of strong combinations at frequencies with simple relationships to their parent modes (such as $2\nu_1$ or $\nu_1 + \nu_2$) argues against this origin (Pápics 2012). The origin of these peaks therefore remains unclear.

#### 5.2.2 *At 0.3 d$^{-1}$ – A Fourier signal of rotation?*

Figure 1 also shows power at 0.3 d$^{-1}$. This is clearer in Fig. 13, where the dipole g modes have been fitted to the light curve and subtracted. There is a broad power excess around 0.3 d$^{-1}$, which could be a signature of the surface rotation of the star. It is flanked by two peaks, at 0.28 and 0.33 d$^{-1}$, which would correspond to periods of 3.57 and 3.0 d, respectively. It is hard to see how this corresponds to our spectroscopic rotation rate except in the very unlikely case of $i \sim 6°$, which is also disfavoured by the g-mode amplitudes.

There is, of course, no physical explanation for why this should correspond to the rotation of the star, in the absence of sun-like starspots. We also mentioned surface spots as a possible explanation for the line asymmetry (Sec. 5.1) but, with the exception of chemically peculiar stars, no strong evidence exists for the presence of spots on the surfaces of early-F stars. Rotation has nonetheless been invoked as the cause of both narrow (Balona 2013) and broad (Balona 2014) peaks at low frequency in the Fourier transforms of A-star light curves. Although we cannot explain the broad signal and its harmonic in Fig. 13, it is not consistent with rotation in this case because the implied rotation period is too short by a factor of ten.

We briefly considered that the broad signal could be caused by binarity, but this hypothesis can be ruled out for a several reasons: strong tidal distortion would result from a close companion with an orbital period of ~3 d, but the amplitude of the broad signal is much lower than that seen in typical ellipsoidal variables (Kirk et al. 2016); the Fourier peaks caused by binaries (which have very constant periods on 4-yr timescales) are typically very sharp; the spectrum shows no evidence of a companion; and, when phased upon the peaks flanking the broad signal, the light curve is non-sinusoidal due to the harmonic of the broad signal. The latter evidence would suggest an eccentric orbit, whereas short orbital periods (i.e. $P_{\rm orb} \sim$ 3 d) usually result in highly circularised orbits (e.g. Debernardi et al. 2000). Further, short-period binaries tend to be synchronously rotating, which recalls the discussion in the last paragraph of the incompatibility of the broad peaks with rotation.

### 5.3 Significance of slow rotation

Our ability to measure core rotation rates in A/F stars from g modes has so far been restricted to slow rotators: 105 d (KIC 11145123, Kurtz et al. 2014), 66 d (KIC 9244992, Saio et al. 2015) and around 10 d (KIC 10080943, Schmid et al. 2015). Here, we have found another slow rotator, with $P_{\rm c} = 27$ d. Yet at spectral types common for $\gamma$ Dor stars, i.e. the early-F stars, the mean surface rotation velocity after statistical correction for inclination is about 150 km s$^{-1}$ (Abt & Morrell 1995), corresponding to surface rotation periods of about 1 d. Uniform rotation would give the core a similar rotation period, but the tendency of the core to spin-up due to contraction reduces the period. There is clearly an observed excess of slowly rotating cores.

This can be explained by an observational selection effect. It is very difficult to measure the frequency splittings of rapid rotators, partly because the splittings are much larger than the period spacings, and partly because both the frequency splittings and period spacings become non-linear when the rotation rate is high.

However, there is also physics that is not yet accounted for in stellar models. One example is horizontal shear, which may drastically alter the propagation and therefore visibility of g modes. If the core were rotating more quickly than the envelope then there may exist a co-rotating zone where the rotation speed is equal to the wave speed of retrograde ($m = -1$) g modes, giving them a frequency close to zero in the reference frame of the star and preventing their propagation or at least reducing their visibilities. Without the retrograde modes, rotational splittings may not be measurable, or the remaining zonal ($m = 0$) and prograde ($m = +1$) modes might be interpreted as an $m = \pm 1$ doublet, from which the inferred rotational frequency would be too low by a factor of two. Thus shear might explain why rotation profiles with cores rotating more quickly than the surface have not been observed.

Viscosity is another important piece of physics. The action of viscosity is to reduce rotation gradients. Stellar models almost always assume an inviscid interior because the viscosity coefficients are unknown. At the molecular level, the inviscid assumption is valid, but turbulent viscosity is non-negligible. Indeed, turbulent pressure contributes as much as 15 per cent of the total pressure in the convective zone of early-F stars (Grassitelli et al. 2015), and the associated viscosity should be accounted for. Perhaps viscosity works efficiently at reducing rotation gradients, and this is why near-uniform rotation profiles tend to be observed, but this requires turbulent motion to be ubiquitous in the radiative layers between the core and the envelope.

Of course there are other angular momentum transport mechanisms to consider, not least of which are magnetic fields, as we mentioned in Sect. 1. Progress in understanding the interiors of early-type main-sequence stars might hinge on theoretical developments along these lines. We are therefore fortunate to have such exquisite photometry to make the supporting observations.

## 6 CONCLUSIONS

By measuring the rotational splittings of a series of dipole g modes in KIC 7661054, we have established its core rotation period to be $P_{\rm c} = 27.25 \pm 0.06$ d. Analysis of spectral line profiles reveals a

similar rotation period for the surface, of $P_s <= 26.7 \pm 4.7$ d, where the inequality represents the upper limit imposed at $\sin i = 1$. We conclude that KIC 7661054 has a nearly uniform rotation profile, with the surface possibly rotating slightly faster than the core.

We have shown that spectral line broadening mechanisms can have a strong impact on derived atmospheric parameters, even in early-F stars, and especially for slow rotators.

We identified a broad signal at low frequency ($\sim 0.3\,\mathrm{d}^{-1}$) in the Fourier transform of the star's light curve, for which we have shown a rotational origin is implausible. This calls into question the hypothesis that rotation is the cause of this type of low-frequency variability in A stars.

The ratio of the core and surface rotation periods, $P_c/P_s >= 1.0 \pm 0.2$, adds another example of near-uniform rotation on the main sequence to the literature. These observational results provide strong evidence for efficient angular momentum transport throughout the stellar lifetime. Continued investigation of the rotation profiles at various ages on the main sequence is required to identify the responsible mechanism(s).

## ACKNOWLEDGEMENTS

We are grateful to the anonymous referee for a most thorough reading of the paper. This research was supported by the Australian Research Council. Funding for the Stellar Astrophysics Centre is provided by the Danish National Research Foundation (grant agreement no.: DNRF106). The research is supported by the ASTERISK project (ASTERoseismic Investigations with SONG and Kepler) funded by the European Research Council (grant agreement no.: 267864).

## REFERENCES

Abt H. A., Morrell N. I., 1995, ApJS, 99, 135
Aerts C., Puls J., Godart M.-A., Dupret M.-A., 2009, A&A, 508, 409
Aerts C., Christensen-Dalsgaard J., Kurtz D. W., 2010, Asteroseismology. Springer
Aerts C., Simón-Díaz S., Groot P. J., Degroote P., 2014, A&A, 569, A118
Asplund M., Grevesse N., Sauval A. J., Scott P., 2009, ARA&A, 47, 481
Balona L. A., 2013, MNRAS, 431, 2240
Balona L. A., 2014, MNRAS, 441, 3543
Barklem P. S., Piskunov N., O'Mara B. J., 2000, A&A, 363, 1091
Beck P. G., et al., 2012, Nature, 481, 55
Bedding T. R., Murphy S. J., Colman I. L., Kurtz D. W., 2015, European Physical Journal Web of Conferences, 101, 1005
Cantiello M., Mankovich C., Bildsten L., Christensen-Dalsgaard J., Paxton B., 2014, ApJ, 788, 93
Canuto V. M., Mazzitelli I., 1991, ApJ, 370, 295
Canuto V. M., Mazzitelli I., 1992, ApJ, 389, 724
Cayrel R., van't Veer-Menneret C., Allard N. F., Stehlé C., 2011, A&A, 531, A83
Charpinet S., Fontaine G., Brassard P., 2009, Nature, 461, 501
De Cat P., Aerts C., 2002, A&A, 393, 965
Debernardi Y., Mermilliod J.-C., Carquillat J.-M., Ginestet N., 2000, A&A, 354, 881
Deheuvels S., et al., 2012, ApJ, 756, 19
Deheuvels S., et al., 2014, A&A, 564, A27
Deheuvels S., Ballot J., Beck P. G., Mosser B., Østensen R., García R. A., Goupil M. J., 2015, A&A, 580, A96
Donati J.-F., Semel M., Carter B. D., Rees D. E., Collier Cameron A., 1997, MNRAS, 291, 658
Eddington A. S., 1926, The Internal Constitution of the Stars
Eff-Darwich A., Régulo C., Korzennik S. G., Pérez Hernández F., Roca Cortés T., 2008, Astronomische Nachrichten, 329, 470
Eggenberger P., Montalbán J., Miglio A., 2012, A&A, 544, L4
Erspamer D., North P., 2003, A&A, 398, 1121
Fossati L., Ryabchikova T., Shulyak D. V., Haswell C. A., Elmasli A., Pandey C. P., Barnes T. G., Zwintz K., 2011, MNRAS, 417, 495
Fuhrmann K., Pfeiffer M., Frank C., Reetz J., Gehren T., 1997, A&A, 323, 909
Fuller J., Lecoanet D., Cantiello M., Brown B., 2014, ApJ, 796, 17
Fuller J., Cantiello M., Stello D., Garcia R. A., Bildsten L., 2015, Science, 350, 423
Gizon L., Solanki S. K., 2003, ApJ, 589, 1009
Grassitelli L., Fossati L., Langer N., Miglio A., Istrate A. G., Sanyal D., 2015, A&A, 584, L2
Gray D. F., 2005, The Observation and Analysis of Stellar Photospheres. Cambridge University Press
Herwig F., 2000, A&A, 360, 952
Keen M. A., Bedding T. R., Murphy S. J., Schmid V. S., Aerts C., Tkachenko A., Ouazzani R.-M., Kurtz D. W., 2015, MNRAS, 454, 1792
Kirk B., et al., 2016, AJ, 151, 68
Kjeldsen H., Bedding T. R., 1995, A&A, 293, 87
Kochukhov O. P., 2007, in Romanyuk I. I., Kudryavtsev D. O., Neizvestnaya O. M., Shapoval V. M., eds, Physics of Magnetic Stars. pp 109–118 (arXiv:astro-ph/0701084)
Kochukhov O., Makaganiuk V., Piskunov N., 2010, A&A, 524, A5
Kupka F., Piskunov N., Ryabchikova T. A., Stempels H. C., Weiss W. W., 1999, A&AS, 138, 119
Kurtz D. W., Saio H., Takata M., Shibahashi H., Murphy S. J., Sekii T., 2014, MNRAS, 444, 102
Kurtz D. W., Shibahashi H., Murphy S. J., Bedding T. R., Bowman D. M., 2015, MNRAS, 450, 3015
Kurucz R., 1993, ATLAS9 Stellar Atmosphere Programs and 2 km/s grid. Kurucz CD-ROM No. 13. Cambridge, Mass.: Smithsonian Astrophysical Observatory, 1993., 13
Lenz P., Breger M., 2004, in J. Zverko, J. Ziznovsky, S. J. Adelman, & W. W. Weiss ed., IAU Symposium Vol. 224, The A-Star Puzzle. CUP, pp 786–790, doi:10.1017/S1743921305009750
Lenz P., Breger M., 2005, Communications in Asteroseismology, 146, 53
Marques J. P., et al., 2013, A&A, 549, A74
Miglio A., Montalbán J., Noels A., Eggenberger P., 2008, MNRAS, 386, 1487
Mosser B., et al., 2012, A&A, 548, A10
Murphy S. J., 2014, PhD thesis, Univ. of Central Lancashire
Murphy S. J., Bedding T. R., Niemczura E., Kurtz D. W., Smalley B., 2015, MNRAS, 447, 3948
Niemczura E., et al., 2015, MNRAS, 450, 2764
Pápics P. I., 2012, Astronomische Nachrichten, 333, 1053
Pápics P. I., Moravveji E., Aerts C., Tkachenko A., Triana S. A., Bloemen S., Southworth J., 2014, A&A, 570, A8
Pápics P. I., Tkachenko A., Aerts C., Van Reeth T., De Smedt K., Hillen M., Østensen R., Moravveji E., 2015, ApJ, 803, L25
Paxton B., et al., 2013, ApJS, 208, 4
Piskunov N. E., Kupka F., Ryabchikova T. A., Weiss W. W., Jeffery C. S., 1995, A&AS, 112, 525
Reiners A., Schmitt J. H. M. M., 2003, A&A, 398, 647
Rogers T. M., Lin D. N. C., McElwaine J. N., Lau H. H. B., 2013, ApJ, 772, 21
Ryabchikova T., et al., 2016, MNRAS, 456, 1221
Saio H., Cox J. P., 1980, ApJ, 236, 549
Saio H., Kurtz D. W., Takata M., Shibahashi H., Murphy S. J., Sekii T., Bedding T. R., 2015, MNRAS, 447, 3264
Schmid V. S., et al., 2015, A&A, 584, A35
Schou J., et al., 1998, ApJ, 505, 390
Shulyak D., Tsymbal V., Ryabchikova T., Stütz C., Weiss W. W., 2004, A&A, 428, 993
Simón-Díaz S., Herrero A., 2014, A&A, 562, A135
Smith J. C., et al., 2012, PASP, 124, 1000
Stępień K., 2000, A&A, 353, 227

Stello D., Cantiello M., Fuller J., Huber D., García R. A., Bedding T. R., Bildsten L., Aguirre V. S., 2016, Nature, 529, 364
Stumpe M. C., et al., 2012, PASP, 124, 985
Tayar J., Pinsonneault M. H., 2013, ApJ, 775, L1
Thompson M. J., Christensen-Dalsgaard J., Miesch M. S., Toomre J., 2003, ARA&A, 41, 599
Triana S. A., Moravveji E., Pápics P. I., Aerts C., Kawaler S. D., Christensen-Dalsgaard J., 2015, ApJ, 810, 16
Tsymbal V., 1996, in Adelman S. J., Kupka F., Weiss W. W., eds, Astronomical Society of the Pacific Conference Series Vol. 108, M.A.S.S., Model Atmospheres and Spectrum Synthesis. p. 198
Unno W., Osaki Y., Ando H., Saio H., Shibahashi H., 1989, Nonradial oscillations of stars. University of Tokyo Press
Van Grootel V., Charpinet S., Fontaine G., Brassard P., Reese D., 2009, Journal of Physics Conference Series, 172, 012072
Van Reeth T., et al., 2015a, ApJS, 218, 27
Van Reeth T., et al., 2015b, A&A, 574, A17
Wolff S. C., 1983, The A-type stars: problems and perspectives.. NASA SP-463
Wolff S., Simon T., 1997, PASP, 109, 759
Zima W., et al., 2006, A&A, 455, 235
Zorec J., Royer F., 2012, A&A, 537, A120
Zwintz K., et al., 2014, Science, 345, 550

## APPENDIX A: THEORETICAL CONVERSION OF LIGHT-AMPLITUDE TO VELOCITY

Kjeldsen & Bedding (1995) derived a relation between light and velocity amplitudes for p modes. The relation is based on the adiabatic relation between temperature ($\delta T/T$) and density perturbations, which are proportional to luminosity perturbation ($\delta L/L$) and radial displacement, respectively. Here, instead of deriving an empirical relation for g modes, we have calculated the ratio of light-amplitude[5] to velocity of each g mode by using the eigenvalue and eigenfunction obtained from a non-adiabatic analysis.

A linear non-adiabatic analysis of non-radial pulsation solves two thermal variables, usually entropy perturbation and $\delta L/L$, in addition to dynamical variables (including pulsational displacements) which appear in an adiabatic analysis. For a pulsation mode, adoption of plane-parallel grey atmospheres leads to $\delta L/L \approx 4\delta T/T$ at the surface (the same relation was used by Kjeldsen & Bedding 1995). In our case, however, non-adiabatic effects are included in $\delta T/T$, and the velocity amplitude is obtained from the corresponding displacement and the pulsation frequency.

Since the amplitudes in the linear analysis are normalized by a quantity (usually by the radial displacement at the surface), each individual amplitude does not represent an actual amplitude, but amplitude *ratios* are free of normalization and can be compared with observations. For g modes, in which horizontal motion dominates (e.g. Unno et al. 1989; Aerts et al. 2010), the amplitude ratio of velocity to light variation corresponds to the ratio of horizontal velocity, which is proportional to the frequency times horizontal displacement, to the luminosity variation at the surface.

We have obtained non-adiabatic eigenfrequencies and eigenfunctions of dipole g modes for our best model (1.9 $M_\odot$) of KIC 7661054, as well as some Slowly Pulsating B (SPB) star models of 4, 5 and 6 $M_\odot$ with $(X, Z) = (0.72, 0.014)$, by using the method given by Saio & Cox (1980). Using the non-adiabatic eigenfunction and the frequency of each g mode in those models, we have derived the ratio of the velocity to light amplitude, which is plotted as a function of frequency in Fig. A1. For the 1.9-$M_\odot$ model, all the dipole g modes in the period range of this figure are plotted (black circles), while only excited modes are plotted for the SPB models (triangles). Also plotted are observational data of SPB stars from De Cat & Aerts (2002) (red squares with error bars). In the frequency range 0.5–0.9 $d^{-1}$, theoretical predictions for SPBs are consistent with observations, while the ratios of longer period SPBs tend to be larger than the theoretical ones.

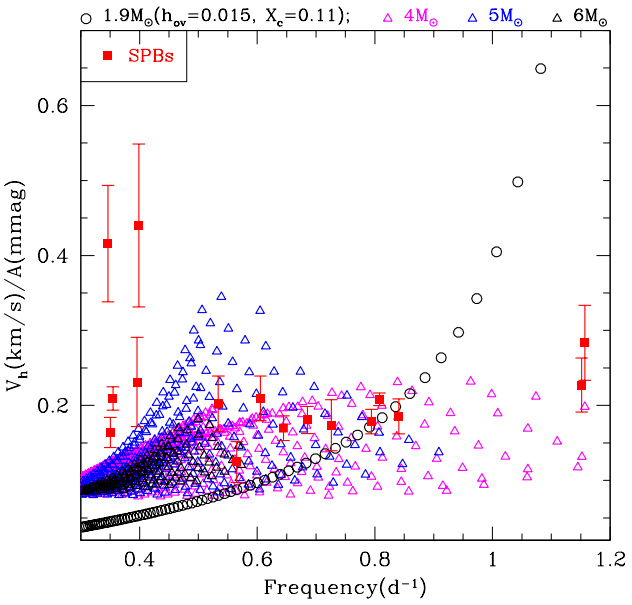


**Figure A1.** The ratio of the horizontal velocity to light amplitude as a function of the pulsation frequency for dipole g modes in our best model of KIC 7661054 (black circles) and models for SPB stars (triangles). For the latter models, only excited dipole modes are plotted. Red squares with error bars are observational data SPB stars from De Cat & Aerts (2002).

Combining observed light amplitudes with the theoretical ratio of velocity to light amplitude as a function of frequency, we have obtained the expected radial velocity amplitude, $V_j$, for each of the 33 observed frequencies in KIC 7661054. Since pulsation phases are random, these radial velocity variations should appear as a contribution to the macroturbulence. The contribution can be estimated by

$$\sqrt{\sum_{j=1}^{33} V_j^2},$$

which we calculate to be 2.3 km $s^{-1}$. If we take into account invisible zonal modes, the number would increase to ($\sqrt{3/2} \times 2.3$ km $s^{-1}$ =) 2.8 km $s^{-1}$, but the total is reduced to around 2 km $s^{-1}$ when the projection effect is accounted for.

This paper has been typeset from a TEX/LATEX file prepared by the author.

[5] This analysis assumes a bolometric light amplitude, but the wavelength for which the observed amplitude equals the bolometric amplitude in a 6800-K star is 530 nm (Kjeldsen & Bedding 1995, equation 4) – which is in the middle of the *Kepler* bandpass.